Comparison of Two Independent Crystal Structures of Human Dihydrofolate Reductase Ternary Complexes Reduced with Nicotinamide Adenine Dinucleotide Phosphate and the Very Tight-Binding Inhibitor PT523[†,‡]

Vivian Cody,*[,§] Nikolai Galitsky,[§] Joseph R. Luft,[§] Walter Pangborn,[§] Andre Rosowsky,[||] and Raymond L. Blakley[⊥]

Hauptman-Woodward Medical Research Institute, Inc., 73 High Street, Buffalo, New York 14203, Department of Biological Chemistry and Molecular Pharmacology, Dana-Farber Cancer Institute and Harvard Medical School, 44 Binney Street, Boston, Massachusetts 02115, and Department of Molecular Pharmacology, St. Jude Children's Hospital, Memphis, Tennessee 38105

Received July 14, 1997; Revised Manuscript Received September 8, 1997[⊗]

ABSTRACT: Structural data for two independent crystal forms (monoclinic, *C*2, and orthorhombic, $P2_12_12_1$) of the ternary complex of the potent antitumor agent PT523 [N^{α}-(4-amino-4-deoxypteroyl)-N^{δ}-hemiphthaloyl-L-ornithine], reduced nicotinamide adenine dinucleotide phosphate (NADPH), and recombinant human dihydrofolate reductase (hDHFR) reveals multiple binding orientations for the hemiphthaloyl group of the inhibitor. Analysis of these data shows that PT523 binds with its pteridine ring in the same orientation observed for methotrexate (MTX) analogues. However, in each structure, the hemiphthaloyl ring occupies three alternate conformations. In the *C*2 lattice, the phthaloyl moiety binds in two extended conformations, A and C, with each conformer having a 180° flip of the *o*-carboxylate group, and a third, lower occupancy conformer B, with the phthaloyl group folded within contact of the active-site pocket. In the orthorhombic lattice, PT523 also has three conformers for the phthaloyl group; however, these differ from those observed in the monoclinic lattice. Two major conformers, A and C, are displaced on either side of the extended position observed in the *C*2 lattice, one near the folded B conformer of the *C*2 lattice and the other extended. These conformers form tighter intermolecular contacts than those in the *C*2 lattice. Conformer B is folded back away from the active site in a unique position. There are also significant differences in the conformation of the adenine−ribose moiety of NADPH in both complexes that differ from that observed for other inhibitor−NADPH−hDHFR ternary complexes. These data suggest that the added intermolecular contacts made by the hemiphthaloyl group of PT523 contribute to its tighter binding to hDHFR than MTX, which does not extend as far from the active site and cannot make these contacts. These crystallographic observations of multiple conformations for the hemiphthaloyl group are in general agreement with solution NMR data for the binding of PT523 to hDHFR [Johnson et al. (1997) *Biochemistry* ***36***, 4399−4411], which show that the hemiphthaloyl group may adopt more than one conformation. However, the crystallographic data reveal more discretely occupied positions than can be interpreted from the solution data. These results suggest that crystal packing interactions may influence their stability.

Numerous analogues of folate substrates of human dihydrofolate reductase (hDHFR), an enzyme required for the synthesis of purines and pyrimidines, have been synthesized and tested as DHFR inhibitors and antitumor agents (*1*−*3*). The ability of the L-glutamate side chain in classical DHFR inhibitors such as methotrexate (MTX) to form polyglutamate conjugates of the γ-carboxy group is a critical determinant of both their potency and therapeutic selectivity (*4*). In an effort to enhance the selectivity and reduce the toxicity of these compounds, in particular MTX, still the most widely used antitumor agent (*4*), compounds that inhibit other folate-dependent enzymes have been studied. Structure−activity relationships among novel compounds that inhibit hDHFR reveal that analogues which modify the γ-glutamate moiety of classical antifolates have the potential to act as dual-function antifolates as they will also inhibit the enzyme folylpolyglutamate synthetase, responsible for polyglutamation of folates in cells (*5*−*8*).

In the course of a systematic exploration of the structure−activity relationships in antifolates, the potent antitumor compound PT523 [N^{α}-(4-amino-4-deoxypteroyl)-N^{δ}-hemiphthaloyl-L-ornithine), a nonpolyglutamatable analogue of MTX was synthesized (*9*) and studied (*10*−*12*) (Figure 1). PT523 was more toxic than MTX against both MTX-resistant and -sensitive cells and was recently reported to bind 15-fold more tightly than methotrexate to recombinant hDHFR (*13*). Further characterization of its properties revealed that the length of the chain between the carboxamide and the position of the aromatic carboxylate group were critical to the solubility for uptake and transport and for increased hydrophobicity of the compound. A major objective in the development of PT523 and related compounds has been to bypass polyglutamation while retaining potent activity against hDHFR (*14*−*16*). Although PT523 binds to DHFR nearly

[†] Supported in part by GM-51670 (V.C.), CA-25394 (A.R.), CA-31922, CA-21765, and American Lebanese Syrian Associated Charities (R.L.B.).

[‡] Coordinates for both structures have been deposited with the Brookhaven Protein Data Bank (codes 1OHJ and 1OHK).

* To whom correspondence should be addressed: email cody@hwi.buffalo.edu.

[§] Hauptman-Woodward Medical Research Institute, Inc.

[||] Dana-Farber Cancer Institute and Harvard Medical School.

[⊥] St. Jude Children's Hospital.

[⊗] Abstract published in *Advance ACS Abstracts,* November 1, 1997.

S0006-2960(97)01711-X CCC: $14.00

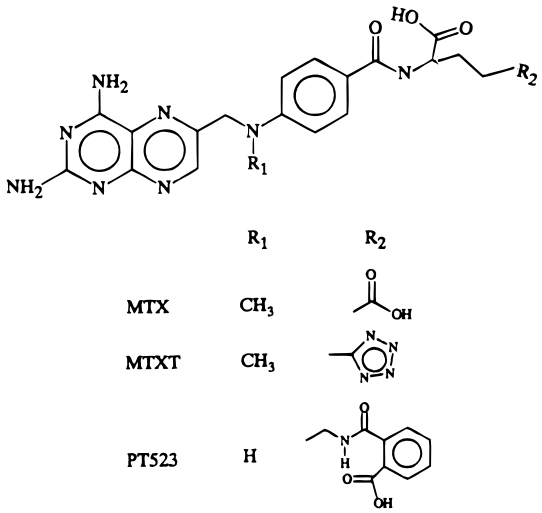

FIGURE 1: Schematic diagram of DHFR inhibitors PT523, MTX, and MTXT.

stoichiometrically, like MTX, its potency as a cell growth inhibitor is substantially greater as it is 10−100-fold more potent than MTX against most cell lines *in vitro* (*9*, *12*, *16*). However, the greater *in vitro* potency relative to MTX cannot be explained simply on the basis of tighter binding to hDHFR. Further modification of PT523 by changing the length of the methylene linker and the position of the aromatic carboxylate revealed that PT523 was the optimized analogue, as these others had reduced effectiveness (*16*).

To investigate the structural basis for the inhibition strength of PT523, multinuclear NMR techniques were used to study binary and ternary complexes of PT523 and NADPH with human DHFR (*13*). These data reveal that the binary complex has two distinct conformations in solution that convert to a single bound state on addition of NADPH. Concurrent with these solution studies, the crystal structure of hDHFR ternary complexes with PT523 was also investigated. The results of two independent crystal structure determinations of ternary complexes of PT523, NADPH, and hDHFR are reported here.

EXPERIMENTAL PROCEDURES

Crystallization and X-ray Data Collection. Wild-type recombinant human DHFR was cloned, isolated, and purified as previously described (*17*). The protein was incubated overnight at 4 °C in a molar excess of NADPH followed by the inhibitor, PT523, which was synthesized as previously described (*9*). Hanging drop vapor diffusion experiments were carried out at 20 °C with various crystallization screens. Two types of crystals were finally obtained over a period of several months of unsuccessful trials. Monoclinic crystals were grown from 40% PEG 4000, 0.2 M sodium acetate, and 0.1 M Tris-HCl, pH 7.0, in the wells and 3 μL of protein solution mixed with 3 μL of well solution in the droplet. Orthorhombic crystals were grown from Hampton Research Screen II, number 23 (Hampton Research, Riverside, CA), which contained 10% dioxane, 0.1 M MES, pH 6.5, and 1.6 M ammonium sulfate in the reservoir.

Data collection was carried out on the best crystals available using a Rigaku RaxisIIc Imaging plate system with a rotating anode source. Diffraction data showed the presence of two crystal forms: a monoclinic lattice, space group $C2$ with cell parameters of $a = 65.82$, $b = 40.35$, and $c = 75.15$ Å with $\beta = 109.74°$, and an orthorhombic lattice, space group $P2_12_12_1$, with cell parameters $a = 36.90$, $b = 69.19$, and $c = 69.95$ Å. This is the first report of hDHFR complexes in these space groups, as previous hDHFR complexes have been reported only in the rhombohedral space group, $R3$ (*17*−*21*), or the triclinic $P1$ lattice (*22*). Diffraction data were collected on the best crystals available to a maximum of 2.5 Å resolution. Crystal lattice properties and data collection statistics are listed in Table 1.

Table 1: Crystal Properties and Refinement Statistics for PT523−NADPH−hDHFR Complexes

	lattice type	
	monoclinic	orthorhombic
lattice constants (Å)	65.82, 40.35, 75.15; $\beta = 109.74$	36.90, 64.19, 69.95
space group	$C2$	$P2_12_12_1$
resolution range (Å)	8.0−2.5	8.0−2.5
reflections used	5976	5293
R factor (%)	19.9	19.8
protein atoms	1592	1592
water molecules	10	18
B factor (protein average) (Å^2)	16.86	19.41

		root mean square deviation	
	target σ	monoclinic	orthorhombic
distances (Å)			
bonds	0.020	0.018	0.019
angles	0.040	0.062	0.063
planar 1−4	0.050	0.057	0.066
nonbonded distances (Å)			
single torsion	0.500	0.251	0.257
planar groups	0.020	0.013	0.014
chiral volume	0.150	0.220	0.221
multiple torsion	0.500	0.313	0.362
possible hydrogen bonds	0.500	0.359	0.362
torsion angles (deg)			
planar	5.0	2.6	2.4
staggered	15.0	23.3	25.9
orthonormal	15.0	19.6	23.8

Structure Determination and Refinement. The structures of both ternary complexes of PT523, NADPH, and hDHFR were solved by molecular replacement methods with the program X-PLOR (*23*) used to orient the enzyme in the $C2$ and $P2_12_12_1$ lattices based on the coordinates of the hDHFR from the methotrexate γ-tetrazole (MTXT) ternary structure (*18*). Refinement was continued using the restrained least-squares program PROLSQ (*24*); modified by G. D. Smith, HWI) in combination with the model-building program CHAIN (*25*). All calculations were carried out on a Silicon Graphics Impact R1000 workstation. The initial $(2|F_o| - |F_c|)\exp i\alpha_c$ maps, where F_o are the observed and F_c the calculated structure factors based on the protein model only and α_c is the calculated phase, resulted in electron density corresponding to both the inhibitor PT523 and the reduced cofactor, NADPH, as well as a good fit of the protein to its density.

Further restrained refinement was continued for the ternary complexes, including the cofactor and inhibitor, which was modeled on that of MTX in which the hemiphthaloyl group was generated using the builder function of Sybyl (*26*) (Figure 1). NADPH was taken from the wild-type ternary structure (*18*). The aromatic rings of PT523 and NADPH were constrained to be planar. Between least-squares minimizations, the structures were manually adjusted to fit

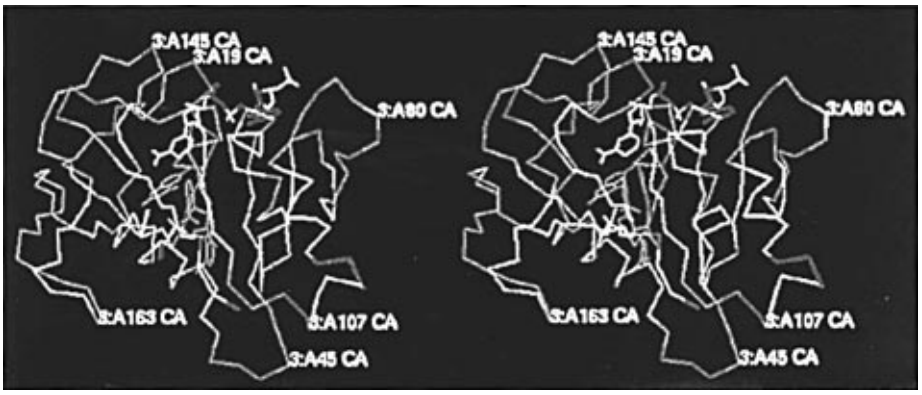

FIGURE 2: α-Carbon trace of hDHFR colored by temperature factor for hDHFR−PT523−NADPH ternary complex in the $P2_12_12_1$ lattice. The highest thermal motions are colored white and the lowest are colored blue. Also labeled are the surface loop regions.

difference electron density and verified by a series of omit maps calculated from the current model with deleted fragments.

In both structures, electron density for the hemiphthaloyl group was poor. When the electron density was fit by a model for one conformer, either extended or folded, the thermal parameters became larger, indicating less occupancy, while at the same time the residual density for the alternative ring positions remained positive and did not behave as solvent. Ultimately, three conformers of the benzoyl ring were modeled to the residual density in a series of disordered positions that were then not refined. The presence of such disordered models was suggested on the basis of solution NMR studies which were on-going during these crystallographic refinements (*13*).

The final refinement statistics are summarized in Table 1. The Ramachandran conformational parameters from the last cycle of refinement for both structures generated by PROCHECK (*27*), shows that between 84% and 87% of the residues in both structures have the most favored conformation and none are in disallowed regions. Coordinates for both structures have been deposited with the Brookhaven Protein Data Bank.

Table 2: PT523 Phthaloyl Group Intermolecular Contacts

	*C*2 lattice		$P2_12_12_1$ lattice	
disorder model	contact	distance (Å)	contact	distance (Å)
A	O41···ND2 Asn-64	5.2	O41···O Arg-28	2.9
	O42···NE Arg-28	4.9	O42···NE Arg-28	3.7
			O42···NE Arg-32	3.5
			O33···O41	2.9
B	O41···NE Arg-28	4.8	O42···Nz Lys-63	2.8
	C···C Pro-26	4.2	C···C Pro-26	4.2
	C···C Phe-31	3.5	C···C Phe-31	3.5
	C···C pABA	3.7	C···CpABA	4.3
	C···C Pro-61	4.2	C···C Pro-61	4.4
C	O41···NE Arg-32	3.0	O41···NE Gln-35	3.0
	O41···NH_2 Arg-32	4.2	O42···OE Gln-35	2.8
	O42···N31 (intra)	2.4	O42···Nz Lys-68	4.1
	O42···NE2 Gln-35	4.6	O33···O41	2.9

RESULTS

Overall Structure. The structures of the two hDHFR−PT523−NADPH ternary complexes were compared with that of hDHFR−MTXT−NADPH (*18*). Analysis of the diffraction data showed that both structures are ternary complexes with NADPH present along with PT523, which binds with its pteridine ring in the same orientation observed for MTXT (*18*). Least-squares superposition of 159 backbone atoms (Profit program, G. D. Smith, HWI Library) showed that the average root mean square deviation in these backbone positions between the *C*2 and the $P2_12_12_1$ complexes was 0.43 Å, while between the *R*3 hDHFR−NADPH−MTXT complex and the *C*2 complex it was 0.30 Å, and between the *R*3 and the $P2_12_12_1$ complexes it was 0.37 Å. These data show that the C2 structure is more similar to that of the MTXT complex, while the orthorhombic structure shows more regions that differ in backbone conformation. There are a number of regions among these structures where the backbone positions differ significantly from one another (i.e., $\approx$ 0.90 Å). As highlighted in Figure 2 for the orthorhombic structure, the regions of largest differences encompass the flexible loop regions between residues 39 and 48, 60 and 65, 93 and 110, and 147 and 159 of the two PT523 complexes. There is also a *cis* peptide linkage between Arg-65 and Pro-66 and between Gly-116 and Gly-117, as observed in other human DHFR complexes (*18*, *19*).

Inhibitor Binding. The binding orientation of the pteridine ring of PT523 in both structures is similar to that observed for MTXT. The carboxylate oxygens of Glu-30 protonate the pteridine ring of PT523, forming hydrogen bonds by OE2 and OE1 to N(1) and the 2-amino group. In addition, the carboxylate oxygens of the glutamate form hydrogen bonds to a conserved Thr-136 and to water (*18*, *19*). There is also well-ordered electron density of PT523 and NADPH.

The most interesting feature of these two crystal structures is the observation of multiple conformers for the hemiphthaloyl group of PT523. As illustrated (Table 2; Figures 3−5), a wide range of intermolecular contacts are accessible to the hemiphthaloyl group. In the *C*2 lattice (Figure 4), the principal hemiphthaloyl conformers (A and C, Table 2) are extended, in a manner similar to MTXT, but the structure is disordered by the ability of the phthaloyl ring to undergo a 180° flip. There are few direct contacts of the carboxylate to the enzyme for these conformers. However, the carboxylate group makes a hydrogen-bond contact to atom NE of Arg-32 and could make contacts to Arg-28 and Arg-32 amines via intervening water molecules (not observed in the electron density maps at this resolution). There is also an intramolecular contact between the phthaloyl amide nitrogen and the *o*-carboxylate group in conformer C.

A third, lower occupancy conformer (B) in which the phthaloyl group is folded back within contact of the active-

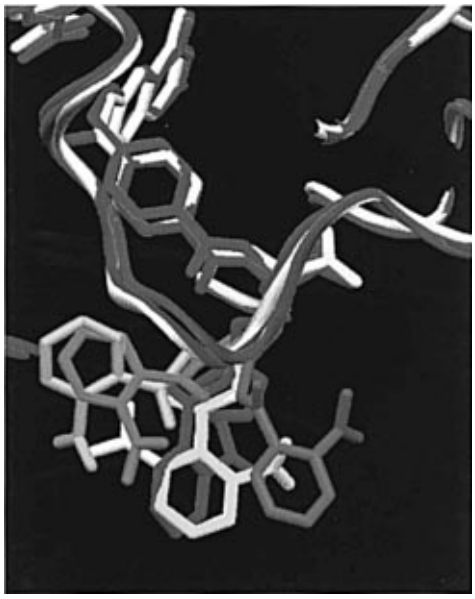

FIGURE 3: Close-up view of the three conformers for the hemiphthaloyl group in PT523 for the *C*2 (A, white; B, gold; C, yellow) and $P2_12_12_1$ (A, violet; B, cyan; C, light blue) lattices. The tetrazole ring of MTXT is colored green. Diagram was made with the program SETOR (*32*).

site pocket can also be interpreted on the basis of electron density maps. In this position the phthaloyl ring occupies a hydrophobic pocket making contacts with Phe-31, Pro-26, Pro-61, and the *p*-aminobenzoyl (pABA) ring of PT523. The carboxylate ring also makes hydrophobic contacts with Pro-128 of a symmetry-related molecule.

There are also multiple conformers for the hemiphthaloyl group of PT523 in the orthorhombic lattice, but these differ from those observed in the monoclinic lattice (Figure 5). Two major conformers (A and C) are displaced from the extended positions (A and C) observed in the *C*2 lattice and, in general, these form closer contacts than in the *C*2 lattice. Conformer A most closely matches the position of conformer C from the *C*2 lattice, while conformer C in the orthorhombic lattice occupies a new position relative to the other complex. These conformers also make close contacts with the enzyme. As illustrated (Table 2), the carboxylate oxygens of conformer A are within hydrogen-bonding contacts with Arg-28 and Arg-32, while the carboxylates of conformer C form close contacts with Glu-35. In this conformation, the carboxamide oxygen (O33) makes a close contact to the amide of Asn-64.

The folded conformer (B) occupies the same hydrophobic pocket observed for conformer B in the *C*2 lattice and makes similar contacts to Pro-26, Pro-61, Phe-31 and the pABA ring of PT523 itself. One of the carboxylate oxygens makes a close contact to Lys-63, not observed in the *C*2 lattice.

NADPH Binding. Although NADPH is bound in an extended conformation, similar to other cofactor complexes (*18*, *19*, *28*−*30*), there is considerable variation in the conformation of the adenine−ribose and the pyrophosphate moieties (Table 3). The conformation of the nicotinamide−ribose moiety in both PT523 complexes is similar to that observed for NADPH in the MTXT complex. However, in the $P2_12_12_1$ lattice there is significant deviation in the conformation of the adenine−ribose moiety. As illustrated (Table 3), the torsion angle about the pyrophosphate bridge (O7−P_a−O8−C11) is extended compared to the *gauche* conformation observed in the *C*2 structure and that of MTXT in the *R*3 lattice. Diffraction data also show that in the $P2_12_12_1$ structure the geometry of the adenine pyrophosphate group (O8−C11−C12−C13) has adopted a *gauche* conformation compared to the extended conformation of the *C*2 and *R*3 structures.

The carboxamide group of the nicotinamide ring, which is *syn* to the nicotinamide ring N, makes a series of strong hydrogen bonds to the conserved residues Ala-9 and Ile-16 in hDHFR. In addition, there are a series of nonbonded C−H···O contacts involving the nicotinamide ring carbons and three neighboring oxygens of residues Leu-7, Ile-16, and Val-115, which lie approximately in the plane of the nicotinamide ring. These features are conserved in all ternary complexes (*18*, *28*).

The intermolecular contacts between the inhibitor, cofactor, and enzyme of these two PT523 complexes are similar to those observed for the MTXT ternary complex (*19*), with the exception of those involving the adenine amino group. In these two PT523 ternary complexes, the change in conformation of the adenine−ribose moiety places the amino of adenine of the orthorhombic lattice within hydrogen-bond contact to Glu-123, whereas in the MTXT complex this contact is much longer. There is also a change in conformation of the ribose hydroxyl O1 in the $P2_12_12_1$ structure, which

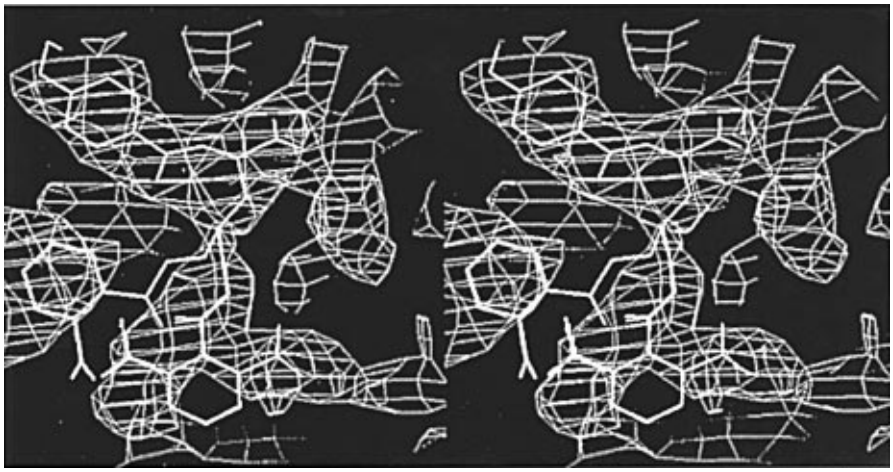

FIGURE 4: Stereo diagram of $2F_0 - F_c$ electron density map, contoured at 1σ, highlighting models for the hemiphthaloyl group for PT523 from *C*2 lattice hDHFR complex (A, white; B, gold; C, yellow).

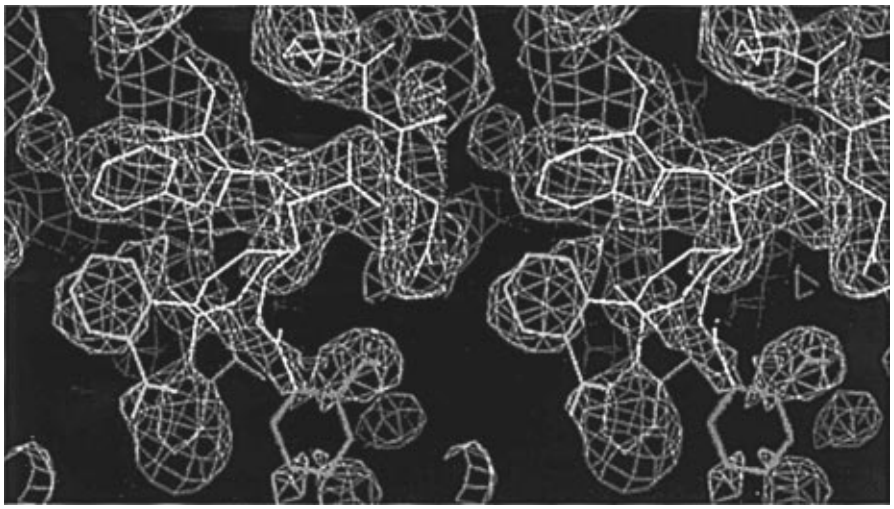

FIGURE 5: Stereo diagram of $2F_o - F_c$ electron density map, contoured at 1σ, highlighting models for the hemiphthaloyl group for PT523 from $P2_12_12_1$ lattice hDHFR complex (A, violet; B, cyan; C, blue).

Table 3: NADPH Conformation in hDHFR Ternary Complexes with PT523 and MTXT

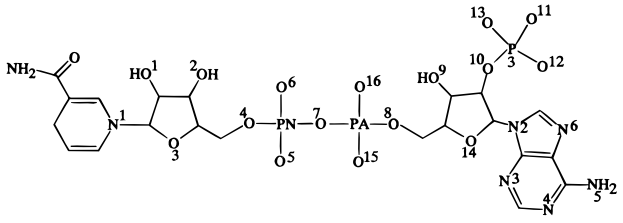

torsion angle[a]		h-MTXT, space group $R3$[b]	h-PT523, space group $C2$	h-PT523, space group $P2_12_12_1$
χ_n	C5−N1−C6−C7	141	132	138
ξ_n	C8−C9−C10−O4	−124	−126	−114
θ_n	C9−C10−O4−P_n	−146	−161	−151
ψ_n	C10−O4−P_n−O7	−52	−67	−56
φ_n	O4−P_n−O7−P_a	123	108	113
φ_a	P_n−O7−P_a−O8	132	155	133
ψ_a	O7−P_a−O8−C11	−82	−83	−174
θ_a	P_a−O8−C11−C12	−147	−156	−176
ξ_a	O8−C11−C12−C13	171	−174	−58
χ_a	C14−C15−N2−C20	−108	−102	−57
θ'_a	C15−C14−O10−P2	153	167	102

[a] subscript n, torsion angles for nicotinamide nucleoside; subscript a, torsion angles for adenine nucleoside; all torsion angles are given in degrees [b] MTXT, methotrexate γ-tetrazole (*18*).

Table 4: Intermolecular Surface Loop Packing Contacts for hDHFR[a]

	$C2$		$P2_12_12_1$		$R3$	
common residue	residue	contact (Å)	residue	contact (Å)	residue	contact (Å)
Asn-19	···Glu-81	4.5	···Ser-42	4.2	···Ser-167	13.4
Gly-45	···Glu-81	3.6	···Val-50	4.9	···Ser-167	11.6
Glu-78	···Arg-32	5.3	···Lys-46	2.7	···Glu-150	3.5
Pro-103	···Leu-99	3.4	···Asn-126	6.6	···Lys-173	9.3
Asp-145	···Lys-173	3.4	···Pro-163	4.3	···Lys-178	4.0
Gly-164	···Tyr-77	3.9	···Glu-143	3.4	···Lys-108	4.4
Ile-175	···Asp-168	7.6	···Asn-29	7.9	···Asn-107	13.7

[a] Residues of surface loops correspond to those illustrated in Figure 2.

places it outside the hydrogen bond contact with Ser-59 observed in other complexes (*17*−*20*).

The distance between the adenine amino group and the nicotinamide moiety has been used as a measure of the extension of the cofactor molecules (*31*). This value is 17.0 and 16.6 Å for the PT523 $C2$ and $P2_12_12_1$ PT523 ternary complexes, respectively, and is shorter than that observed in the MTXT complex (18.0 Å).

Despite these changes in NADPH conformation, the adenine ribose ring adopts a C2′-*endo* conformation and the nicotinamide ribose ring adopt a C3′-*endo* conformation, as observed in other hDHFR complexes. The bases are both *anti* ($\chi = \pm 100-135°$) with respect to the glycosidic linkage in all DHFR structures (Table 3). The adenine ribose 2′-phosphate group fits into a pocket surrounded by charged or polar residues. The positively charged Lys-54 in hDHFR is involved in potential electrostatic interactions to the negatively charged phosphate group. Contacts to Lys-54, Ser-76, Glu-78, and the backbone of Arg-77 in the human structures anchor the phosphate group into position. The binding of the pyrophosphate bridge region is situated between the amino ends of helices of the NADPH binding domain and makes close contacts to Gly-116 and Gly-117, which has a *cis* conformation. The other side of the adenine ring is in contact with the side chain of Lys-55 of the human enzyme.

Packing Analysis. The observation of two independent crystal structures for the ternary complex of hDHFR with NADPH and the inhibitor, PT523, provides an opportunity to compare the influence of packing interactions on the conformations of surface loops in these structures. Figure 2 illustrates the regions of mobility for the orthorhombic structure in which the highest thermal motion of the backbone atoms are white and blue the least. The $C2$ structure has the lowest overall thermal motion while the $R3$ structure has the greatest degree of flexibility. Although there are several regions of conserved thermal motion among these three structures, some flexible regions in one structure become more stable as a result of close intermolecular contacts in different packing environments. Changes in surface contacts that results from crystal packing differences are shown in Table 4, which highlights those residues for the flexible loop regions defined in Figure 2 for the orthorhombic lattice. The regions of highest thermal motion in the $R3$ lattice are surrounded by large open spaces, as indicated by the large contact distances to the neighboring symmetry-related molecules. The $C2$ lattice has the closest packing contacts as

Table 5: Closest Intermolecular Contacts (Less Than 3.2 Å) for hDHFR

*C*2 lattice intermolecular contact residues	$P2_12_12_1$ lattice intermolecular contact residues	*R*3 lattice intermolecular contact residues
Lys-18···Glu-150	Arg-32···Gln-140	Asn-19···Leu-159/ Pro-160
Asn-19···Lys-157	Ser-42···Lys-55	Gln-47···Glu-161
Arg-32···Asp-186	Lys-63···Lys-157	Gly-69···Glu-161
Phe-58···Asn-185	Gly-69···Tyr-156	Gln-78···Glu-150
Glu-62···Leu-159	Arg-77···Gln101	Glu-81···His-130
Lys-80···Asn-107	Lys-80···Pro-128/ Asp-186	Pro-83···Glu-154
His-87···Lys-108	Glu-81···Asp-141	Gln-84···Glu-154/ Asn-185
Ser-90···Glu-104	Ala-86···Pro-160	Gly-85···Gln-183
Gln-102···Gln-102	His-87···Leu-158	
Glu-143···Glu-150	Gln-143···Gly-164 Leu-166···Lys-173	

reflected by the short intermolecular distances present on all surfaces. The $P2_12_12_1$ lattice is also closely packed, but not as tightly as the *C*2 arrangement.

The closest intermolecular contacts for hDHFR among the two PT523 complexes and that of MTXT are listed in Table 5. The packing orientation of DHFR in the *C*2 lattice is such that the inhibitor−cofactor is aligned head (adenine of NADPH)-to-tail (phthaloyl ring of inhibitor) along the crystallographic *y* axis. In the $P2_12_12_1$ lattice, the enzyme molecules are oriented in such a way that the inhibitor−cofactor is aligned head-to-head along the crystallographic *y* axis. In the *R*3 lattice observed for the MTXT ternary complex with hDHFR (*18*), there are large open spaces near the active-site entrance. Therefore, Arg-32 makes good hydrogen-bond contacts in the *C*2 and $P2_12_12_1$ lattices, whereas in the *R*3 lattice it is more flexible as it faces a large solvent channel. Similarly, the more flexible loop encompassing Ser-42 in the *R*3 lattice forms a good intermolecular contact in the $P2_12_12_1$ lattice.

DISCUSSION

Structure−function data for the inhibition of DHFR activity have revealed that the novel antifolate PT523, a nonglutamatable classical analogue of MTX, binds 15-fold more tightly to DHFR than MTX (*13*). Furthermore, this potent antitumor antifolate is 9-fold more potent than MTX against a broad variety of tumor cell lines in culture (*9*−*12*, *16*). This higher potency appears to be due to a combination of tighter binding to hDHFR and more efficient cellular uptake, both of which may be aided by the greater hydrophobicity of the hemiphthaloyl ornithine side chain relative to the glutamate side chain of classical antifolates.

The lower K_i value for PT523 as a DHFR inhibitor is likely to be a direct result of favorable contacts of the hemiphthaloyl group that are not present in MTX. The optimization of these contacts by the *o*-carboxylate substitution pattern of PT523 is highlighted by the weaker DHFR inhibitory activity of the recently described *m*- and *p*-carboxylate analogues (*16*). In addition, the *meta* and *para* analogues of PT523 were shown to have 10- and 240-fold less cytotoxicity than PT523. These data suggest that the aromatic carboxylate group plays a role other than merely increasing water solubility.

The unique features of these diffraction data are the observation of two independent crystal lattices and significant conformational flexibility for the hemiphthaloyl ornithine side-chain group. These crystallographic studies are also the first instance of significant differences in the conformation of the cofactor NADPH adenine−ribose moiety. The observation of several disordered conformers for the hemiphthaloyl group implies that these conformers are of equal energy. That each conformer exploits favorable intermolecular interactions with the enzyme suggests that this may be one of the reasons for the tighter binding than MTX, which cannot make such intermolecular contacts.

In order to understand the structural interactions that could result in the lowered binding affinity for the *m*- and *p*-carboxylate analogues of PT523 (*16*), molecular modeling experiments were also carried out for these analogues in each structure of PT523. In each case, the new analogue was positioned in each of the disordered conformers and its intermolecular contacts noted.

For example, in the *C*2 lattice the *m*-carboxylate makes no unfavorable contacts for either of the two extended conformers A and C. However, in the folded conformer B, one orientation of the *m*-carboxylate ring places the hydrophilic groups too close to the hydrophobic pocket. In the other orientation, the carboxylate group points toward hydrophilic groups. In the *p*-carboxylate PT523 models, short intermolecular contacts to Pro-128 of a symmetry-related molecule were noted.

Examination of the contacts for the *m*-carboxylate PT523 analogue in the $P2_12_12_1$ lattice showed that there are no close intermolecular contacts for the C conformer, but the *m*-carboxylate could form good hydrogen-bonding contacts to Lys-63 and Asn-64 in conformer A. There are no unfavorable contacts for the *p*-carboxylate group. The B conformer results in the same type of interactions observed in the *C*2 lattice while there are no unfavorable contacts for the A conformer. These modeling studies do not reveal a structural reason for the loss of inhibitory potency for these analogues, and one is led to suspect that their lower cytotoxicity may be due to decreased cellular uptake (*16*)

A comparison of the solution and solid-state structures of the ternary complex with PT523 and NADPH shows general agreement. Analysis of the solution conformation of the antitumor drug PT523 by multinuclear NMR techniques indicates that the binary inhibitor complex has two distinct conformations that are in slow exchange (*13*). The addition of NADPH stabilizes the ternary complex in a single bound state. The NMR data further indicated that the largest chemical shift differences were confined to small regions of the ternary enzyme structure and that the pteridine and pABA rings of PT523, as well as the nicotinamide−ribose rings of NADPH, occupied well-defined positions in solution, whereas the position of the hemiphthaloyl group was less well-defined and more than one conformation could exist. The primary solution conformation of the hemiphthaloyl group most closely resembles the folded conformer B in both crystal structures.

Comparison of the packing in each lattice reveals that, in the *C*2 lattice, Arg-32 makes a close contact to the C-terminal residue Asp-186 and the molecules are packed around a 2-fold axis in a head-to-tail manner. However, in the orthorhombic lattice Arg-32 makes close contacts to Asn-140 and Asp-141 and the DHFR molecules are packed around a 2-fold axis in a head-to-head manner. In the more frequently observed *R*3 lattice for hDHFR complexes there

are large open spaces near the active-site entrance and between molecules, with residue Arg-32 near the folate terminus packed around the 3-fold axis. The observation of several discrete conformers in the crystal structure suggests that the crystal packing interactions may influence their stability relative to the solution NMR data. These differences in contact surfaces, along with the added intermolecular binding contacts, may aid in the higher binding affinity for this antifolate. In summary, these data are the first to define discrete conformational flexibility of the hemiphthaloyl group of the potent antitumor agent PT523, as observed in two independent crystal lattices.

ACKNOWLEDGMENT

V.C. thanks Dave Pawlowski and Daniel Cotter for crystal growth experiments.

REFERENCES

1. Blakley, R. L., and Benkovic, S. J. (1984) *Folates and Pteridines*, Vol. 1, John Wiley & Sons, New York.
2. Rosowsky, A. (1989) *Prog. Med. Chem. 26*, 1−252.
3. Blakley, R. L. (1995) *Advances in Enzymology and Related Areas of Molecular Biology* (Meister, A., Ed.) Vol. 70, pp 23−102, John Wiley & Sons, Inc., New York.
4. Bertino, J. R. (1990) *J. Clin. Pharmacol. 30*, 291−295.
5. Rosowsky, A., Forsch, R. A.,Freisheim, J. H., Moran, R. G., and Wick, M. (1984) *J. Med. Chem. 27*, 600−604.
6. Rosowsky, A., Freisheim, R. H., Moran, R. G., Solan, V. C., Bader, H., Wright, J. E., and Radike-Smith, M. (1986) *J. Med. Chem. 29*, 655−660.
7. Rosowsky, A., Moran, R. G., Forsch, R. A., Radike-Smith, M., Colman, P. D., Wick, M. M., and Freisheim, J. H. (1986) *Biochem. Pharmacol. 35*, 3327−3333.
8. McGuire, J. J., Russell, C. A., Balonowska, W. E., Freitag, C. M., Jonas, C. S., & Kalman, T. I. (1990) *Cancer Res. 50*, 1720−1731.
9. Rosowsky, A., Bader, H., Cucchi, C. A., Moran, R. G., Kohler, A., and Freisheim, J. H. (1988) *J. Med. Chem. 31*, 1332−1337.
10. Rhee, M. S., Galivan, J., Wright, J. E., and Rosowsky, A. (1994) *Mol. Pharmacol. 45*, 783−791.
11. Chen, G., Wright, J. E., and Rosowsky, A. (1995) *Mol. Pharmacol. 48*, 758−765.
12. Westerhof, G. R., Schornagel, J. H., Kathmann, I., Jackman, A. L., Rosowsky, A., Forsch, R. A., Hynes, J. B., Boyle, F. T., Peters, G. J., Pinedo, H. M., and Jansen, G. (1995) *Mol. Pharmacol. 48*, 459−471.
13. Johnson, J. M., Meiering, E. M., Wright, J. E., Pardo, J., Rosowsky, A., and Wagner, G. (1997) *Biochemistry 36*, 4399−4411.
14. Rosowsky, A., Bader, H., and Freisheim, J. H. (1991) *J. Med. Chem. 34*, 574−579.
15. Rosowsky, A., Bader, H., Wright, J. E., Keyomarsi, K., and Matherly, L. H. (1994) *J. Med. Chem. 37*, 2167−2174.
16. Rosowsky, A., Vaidya, C. M., Bader, H., Wright, J. E., and Teicher, B. A. (1997) *J. Med. Chem. 40*, 286−299.
17. Chunduru, S. K., Cody, V., Luft, J. R., Pangborn, W., Appleman, J. R., and Blakley, R. L. (1994) *J. Biol. Chem. 269*, 9547−9555.
18. Cody, V., Luft, J. R., Ciszak, E., Kalman, T. I., and Freisheim, J. H. (1992) *Anticancer Drug Des. 7*, 483−491.
19. Cody, V., Wojtczak, A., Kalman, T. I., Freisheim, J. H., and Blakley, R. L. (1993) *Chemistry and Biology of Pteridines and Folates* (Ayling, J. E., Nair, M. G., and Baugh, C. M., Eds.) pp 481−486, Plenum Press, New York.
20. Lewis, W. S., Cody, V., Galitsky, N., Luft, J. R., Pangborn, W., Chunduru, S. K., Spencer, H. T., Appleman, J. R., and Blakley, R. L. (1995) *J. Biol. Chem. 270*, 5057−5064.
21. Oefner, C., D'Arcy, A., and Winkler, F. K. (1988) *Eur. J. Biochem. 174*, 377−385.
22. Davies, J. F., Delcamp, T. J., Prendergast, N. J., Ashford, V. A., Freisheim, J. H., and Kraut, J. (1990) *Biochemistry 29*, 9467−9479.
23. Brunger, A. T. (1992) *XPLOR*, Yale University Press, New Haven, CT.
24. Hendrickson, W. A., and Konnert, J. H. (1980) in *Computing in Crystallography* (Diamond, R., Ramaseshan, S., and Venkatesan, K., Eds.) p 13.01, Indian Academy of Sciences, Bangalore, India; Finzel, B. C. (1987) *J. Appl. Crystallogr. 20*, 53.
25. Sack, J. S. (1988) *J. Mol. Graphics 6*, 224−225.
26. Tripos, St. Louis, MO.
27. Laskowski, R. A., MacArthur, M. W., Moss, D. S., and Thornton, J. M. (1993) *J. Appl. Crystallogr. 26*, 283−291.
28. Bolin, J. T., Filman, S. J., Matthews, D. A., Hamlin, R. C., and Kraut, J. (1982) *J. Biol. Chem. 257*, 13650−13662.
29. Filman, D. S., Bolin, J. T., Matthews, D. A., and Kraut, J. (1982) *J. Biol. Chem. 257*, 13663−136672.
30. Kraut, J., and Matthews, D. A. (1987) in *Biological Macromolecules and Assemblies* (Jurnak, F., and McPherson, A., Eds.) Vol. III, pp 1−71, John Wiley and Sons: New York.
31. Rossmann, M. G., Liljas, A., Branden, C. I., and Banaszak, L. J. (1975) *Enzymes 11*, 61−102.
32. Evans, S. V. (1993) *SETOR*, *J. Mol. Graphics 11*, 148−153.

BI971711L